Extragalactic Fields Optimized for Adaptive Optics

Ivana Damjanov,[1] Roberto G. Abraham,[1] Karl Glazebrook,[2] Peter McGregor,[3] Francois Rigaut,[4] Patrick J. McCarthy,[5] Jarle Brinchmann,[6,7] Jean-Charles Cuillandre,[8] Yannick Mellier,[9] Henry Joy McCracken,[9] Patrick Hudelot,[9] and David Monet[10]

ABSTRACT. In this article we present the coordinates of 67 $55' \times 55'$ patches of sky that have the rare combination of both high stellar surface density (≥ 0.5 arcmin^{-2} with $13 < R < 16.5$ mag) and low extinction ($E(B-V) \lesssim 0.1$). These fields are ideal for adaptive-optics-based follow-up of extragalactic targets. One region of sky, situated near Baade's Window, contains most of the patches we have identified. Our optimal field, centered at R.A.: $7^h24^m3^s$, decl.: $-1°27'15''$, has an additional advantage of being accessible from both hemispheres. We propose a figure of merit for quantifying real-world adaptive optics performance and use this to analyze the performance of multiconjugate adaptive optics in these fields. We also compare our results with those that would be obtained in existing deep fields. In some cases adaptive optics observations undertaken in the fields given in this article would be orders of magnitude more efficient than equivalent observations undertaken in existing deep fields.

Online material: color figures

1. INTRODUCTION

Our understanding of the high-redshift universe has been revolutionized by deep fields, several of which have been extensively surveyed at all accessible wavelengths. Figure 1 shows an up-to-date summary of the locations of all existing deep fields (*circles*). These fields have been primarily used to study galaxy formation and evolution out to very high redshifts (Cowie et al. 1995; Yee et al. 2000; Labbé et al. 2003; Bell et al. 2004; Egami et al. 2004; van Dokkum et al. 2004; Arnouts et al. 2007; Davis et al. 2007; Scoville et al. 2007; Bouwens et al. 2010; Ono et al. 2010). Because galaxies at such high redshifts are typically $<1''$ in size, kinematical investigations of

galaxies in these fields require adaptive optics (AO) spectroscopy (Law et al. 2009; Förster-Schreiber et al. 2009). The promise of such observations has been held out as an exciting next step for over a decade (e.g., Ellis et al. 1997). Unfortunately, it is now clear that only very limited AO observations are going to be undertaken in any existing deep fields.

Coupling integral-field spectroscopy to AO is crucial for understanding the formation of massive galaxies, particularly disks, since at high redshift it has proven difficult for slit spectroscopy to reliably identify kinematic disks, as kinematic and morphological axes are not necessarily correlated (Erb et al. 2006). Even at intermediate redshift ($z \sim 0.6$), it has been demonstrated that galaxies are already kinematically complex and that 3D integral-field spectroscopy (IFS) is essential to physical understanding and kinematic modeling (Rix et al. 1997; Flores et al. 2006). At the highest redshifts AO IFS observations by some groups have given different results compared with non-AO observations of other groups. For example, laser guide star AO observations with kiloparsec resolution (Law et al. 2009) show that $z = 2$–3 Lyman break selected galaxies have high intrinsic velocity dispersions and no significant rotational gradients about a preferred kinematic axis (Law et al. 2009). Förster-Schreiber et al. (2009) found similarly high-velocity dispersions but a much greater incidence of disk rotation in a predominantly non-AO data set of predominantly near-IR selected galaxies. It remains inconclusive whether such differences arise from a difference in sample (massive versus low-mass galaxies) or the fact that the non-AO data has seven-times-poorer resolution, on average, in natural seeing. This is an important question: physical differences in kinematics at

[1] Department of Astronomy & Astrophysics, University of Toronto, 50 St. George Street, Toronto, ON, M5S 3H4 Canada.

[2] Centre for Astrophysics and Supercomputing, Swinburne University of Technology, 1 Alfred Street, Hawthorn, Victoria 3122, Australia.

[3] Research School of Astronomy and Astrophysics, Institute of Advanced Studies, The Australian National University, Canberra, ACT, Australia.

[4] Gemini Observatory, Southern Operations Center, c/o AURA, Casilla 603, La Serena, Chile.

[5] Observatories of the Carnegie Institution of Washington, 813 Santa Barbara Street, Pasadena, CA 91101.

[6] Sterrewacht Leiden, P.O. Box 9513 NL-2300 RA Leiden, The Netherlands.

[7] Centro de Astrofísica, Universidade do Porto, Rua das Estrelas, 4150-762 Porto, Portugal.

[8] Canada-France-Hawaii Telescope Corporation, 65-1238 Mamalahoa Highway, Kamuela, HI 96743.

[9] Institut d'Astrophysique de Paris, UMR7095 CNRS, Université Pierre et Marie Curie, 98 bis Boulevard Arago, 75014 Paris, France.

[10] The United States Naval Observatory, 3450 Massachusetts Avenue, NW, Washington, DC 20392-5420.

		Form Approved OMB No. 0704-0188
	Report Documentation Page	

Public reporting burden for the collection of information is estimated to average 1 hour per response, including the time for reviewing instructions, searching existing data sources, gathering and maintaining the data needed, and completing and reviewing the collection of information. Send comments regarding this burden estimate or any other aspect of this collection of information, including suggestions for reducing this burden, to Washington Headquarters Services, Directorate for Information Operations and Reports, 1215 Jefferson Davis Highway, Suite 1204, Arlington VA 22202-4302. Respondents should be aware that notwithstanding any other provision of law, no person shall be subject to a penalty for failing to comply with a collection of information if it does not display a currently valid OMB control number.

1. REPORT DATE **31 MAR 2011**	2. REPORT TYPE	3. DATES COVERED **00-00-2011 to 00-00-2011**

4. TITLE AND SUBTITLE **Extragalactic Fields Optimized For Adaptive Optics**	5a. CONTRACT NUMBER
	5b. GRANT NUMBER
	5c. PROGRAM ELEMENT NUMBER
6. AUTHOR(S)	5d. PROJECT NUMBER
	5e. TASK NUMBER
	5f. WORK UNIT NUMBER
7. PERFORMING ORGANIZATION NAME(S) AND ADDRESS(ES) **U.S. Naval Observatory,3450 Massachusetts Ave, N.W.,Washington,DC,20392**	8. PERFORMING ORGANIZATION REPORT NUMBER
9. SPONSORING/MONITORING AGENCY NAME(S) AND ADDRESS(ES)	10. SPONSOR/MONITOR'S ACRONYM(S)
	11. SPONSOR/MONITOR'S REPORT NUMBER(S)

12. DISTRIBUTION/AVAILABILITY STATEMENT
Approved for public release; distribution unlimited

13. SUPPLEMENTARY NOTES
Publications of the Astronomical Society of the Pacific Vol. 123, No. 901 (March 2011), pp. 348-365

14. ABSTRACT
In this paper we present the coordinates of 67 55' x 55' patches of sky which have the rare combination of both high stellar surface density (>0.5 arcmin^{-2} with $13<R<16.5$ mag) and low extinction ($E(B-V)<0.1$). These fields are ideal for adaptive-optics based follow-up of extragalactic targets. One region of sky, situated near Baade's Window, contains most of the patches we have identified. Our optimal field, centered at RA: 7h24m3s, Dec: -1deg27'15'', has an additional advantage of being accessible from both hemispheres. We propose a figure of merit for quantifying real-world adaptive optics performance, and use this to analyze the performance of multi-conjugate adaptive optics in these fields. We also compare our results to those that would be obtained in existing deep fields. In some cases adaptive optics observations undertaken in the fields given in this paper would be orders of magnitude more efficient than equivalent observations undertaken in existing deep fields.

15. SUBJECT TERMS

16. SECURITY CLASSIFICATION OF:			17. LIMITATION OF ABSTRACT	18. NUMBER OF PAGES	19a. NAME OF RESPONSIBLE PERSON
a. REPORT **unclassified**	b. ABSTRACT **unclassified**	c. THIS PAGE **unclassified**	**Same as Report (SAR)**	**10**	

high redshift may diagnose the prevalence of fast gas accretion along cold flows in the early universe (e.g., Bournaud et al. 2007), but they may also arise from sample selection effects or observational limitations (for example, Green et al. 2010 suggest that it is simply the high star-formation rates that drive the large velocity dispersions). Most IFS observations at high redshift are still done without AO, due to the technical difficulties of AO and also to the practical difficulties of finding enough targets near sufficiently bright stars in existing deep field samples.

The next stage in the development of this field is to complement kinematical studies by probing chemical abundance gradients at a subkiloparsec scale in star-forming galaxies and to extend existing kinematical investigations to encompass more representative galaxies. This requires AO systems to be operating more efficiently (i.e., without performance limitation imposed by natural guide star availability) and, ultimately, to multiplex if truly large samples are to be obtained. A step in this direction is already being taken with the MASSIV (Mass Assembly Survey with SINFONI in VVDS) survey on the VLT, which targets star-forming galaxies in the redshift range $1 < z < 2$ with SINFONI (Epinat et al. 2009; Queyrel et al. 2009). The targets are more representative than those being probed by Supernova Intensive Studies (SINS), with median stellar masses of $\sim 10^{10}\ M_\odot$ and median star-formation rates of $\sim 10\ M_\odot\,\mathrm{yr}^{-1}$ (the corresponding values for SINS are $\sim 10^{10.5}\ M_\odot$ and $\sim 30\ M_\odot\,\mathrm{yr}^{-1}$, respectively). However, most of the SINFONI data acquired during the MASSIV survey are seeing-limited leading to a final median spatial resolution of ~ 0.6–$0.7''$ with only 25% of the MASSIV sample presently being observed with adaptive optics. Of these AO targets, only a few are being acquired with the smallest pixel size ($0.05''$). The main reasons are (1) the limitations in the availability of natural guide stars, which precludes usefully observing at finer available pixel scale, and (2) the difficulty of reaching the depth required to probe the low-surface brightness component of galaxies in a reasonable exposure time with the smallest pixel size. This latter point leads to expectations of considerable progress in this subject with the advent of 30 m class extremely large telescopes (ELTs).

A basic problem with undertaking AO in existing deep fields, even with laser guide stars, is that one still needs at least one reasonably proximate natural guide star to supply the information needed for tip-tilt correction (Rigaut & Gendron 1992). In contrast, two of the main selection criteria when identifying deep fields have been that they contain as few bright stars as possible to avoid light scattering contamination and saturation in long exposures and that they lie in regions of low Galactic extinction (e.g., Alcalá et al. 2004). Thus, all existing deep fields are near the Galactic poles, where the density of suitable natural guide stars is near a minimum. For example, Davies et al. (2008) report that only 1% of the Lyman break galaxy sample of Mannucci (2007) is accessible to the VLT laser guide star sys-
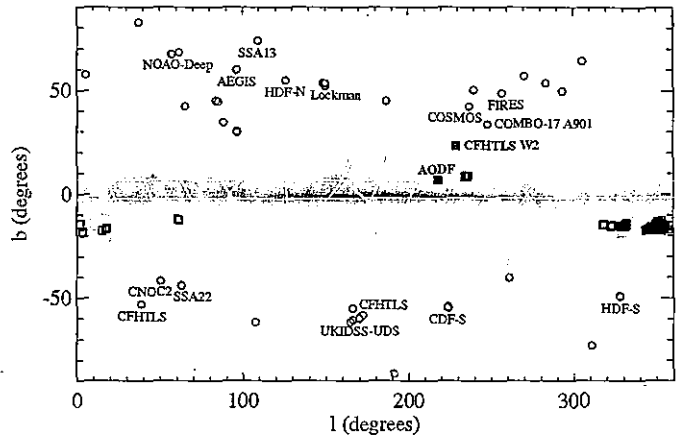

FIG. 1.—Galactocentric coordinates of existing deep fields (*circles*) and the locations of the fields better suited for AO observations presented in Table 1 (*squares*); see § 3 for details. The location of the fields has been overplotted on the dust emission map from the Schlegel et al. (1998) study. Labeled existing deep fields are indicated with filled circles. One labeled square denotes a 1 deg^2 region within the CFHTLS W2 field (§ 5.2). The field labeled AODF is our suggested optimal field whose properties are studied in detail in §§ 4 and 5. See the electronic edition of the *PASP* for a color version of this figure.

tem (Bonaccini et al. 1999): the loss of 75% of the targets is due to the absence of suitably close natural guide stars (NGSs), while an additional 25% are lost after suitable color cuts and elimination of systems at redshifts obscured by strong OH features. The situation is similar with Gemini, whose AO system has similar sky coverage (Ellerbroek & Tyler 1998). Even with the upcoming Gemini multiconjugate AO system (MCAO), the H-band sky coverage at the Galactic poles will only be around 15% (Rigaut et al. 2000), and large benefits for MCAO emerge from having more than the minimum number of natural guide stars. This is because the geometry of the guide stars on the sky impacts the uniformity of the Strehl ratio (Flicker & Rigaut 2001).

The issue of guide star rarity in deep fields becomes prominent in cases where target source density is low. This is often the case for extragalactic programs that focus on unusual objects. For example, many of the key projects described in the *James Webb Space Telescope* (*JWST*) Design Reference Mission (Gardner et al. 2006) rely on either extreme depth or serendipitous lines of sight. If such *JWST* observations are to be synergistic with ground-based AO follow-up, in particular, with next-generation telescopes like the Thirty Meter Telescope (TMT) or the European Extremely Large Telescope (E-ELT), they cannot be undertaken efficiently in any existing deep field. It would be disappointing indeed if only 1%–10% of rare targets imaged with *JWST* in a deep field could be followed up with ground-based integral-field units (IFUs). It is becoming clear that existing and planned AO systems are set to enable transformative high-redshift science, but they will do so only in the regions of the sky in which they are effective.

It is arguable that no existing deep field is suitable for efficient extragalactic AO work (though, of course, the cost of obtaining ancillary data equivalent to that already obtained in existing deep fields may overwhelm the gains obtained from high-efficiency adaptive optics).

In this article we report on the results we have obtained in searching for those fields on the sky most suitable for high-efficiency extragalactic adaptive optics observations. In § 2 we describe the important characteristics of deep fields in the context of adaptive optics observations, such as the acceptable level of dust extinction, field size, and magnitude range of natural guide stars. In § 3 we describe our attempts to identify the most suitable areas on the sky for undertaking extragalactic AO work, which is based on the strategy of combining information from all-sky stellar density and extinction maps. Our preferred AO-friendly field and its first imaging results are described in § 4. In § 5 we define a figure of merit for adaptive optics and use this to compare the efficiency of AO observing in the proposed fields with the efficiency in representative deep fields. Our conclusions are summarized in § 6. All magnitudes in this article are based on the Vega system.

2. DESIRABLE CHARACTERISTICS OF EXTRAGALACTIC FIELDS OPTIMIZED FOR ADAPTIVE OPTICS

In this section we consider the desirable characteristics of extragalactic fields optimized for adaptive optics. The relevant considerations include the maximum acceptable level of extinction from the intergalactic medium, the minimum useful area on the sky, and number density and magnitude range of available natural guide stars. We will consider each of these factors in turn and discuss the importance of each of these factors using very general principles, in order to look for considerations that will remain relevant for future AO systems.

2.1. Extinction

Although most adaptive optics is undertaken in the near-infrared where extinction is lower than at visible wavelengths, it is clear that for any number of reasons, including reliability of photometric redshifts and "future-proofing" the fields so as to make them useful when AO work moves to shorter wavelengths, the ideal fields will lie in regions of low Galactic extinction. As any glance at the night sky will attest, patchy extinction can be rather high in regions with high star counts. It is therefore important to define an upper limit to the acceptable extinction in order to exclude unsuitable fields. A value of $E(B - V) \sim 0.15$ mag is a good starting point, because Fukugita et al. (2004) and Yasuda et al. (2007) show that Galactic extinction estimates become fairly unreliable in regions with $E(B - V) \gtrsim 0.15$ mag. To err on the conservative side, in this article we will use an upper limit of $E(B - V) = 0.1$ mag on the mean extinction as a constraint when exploring star-

count surface density maps for suitable fields. We note that $E(B - V) = 0.1$ mag corresponds to $A_V = R_V \times E(B - V) \sim 0.3$ mag at visible wavelengths and that this is a factor of 3 to 10 times higher than the corresponding extinction in near-infrared (NIR) passbands used by current AO systems.

2.2. Field Size

The next factor to consider is the required size of the field. For extragalactic fields, the area of the field is driven by a desire to minimize the impact of cosmic variance, because scale-dependent inhomogeneity is often the dominant source of error in measurements derived from galaxy populations within a survey volume. The survey volume naturally depends on the area on the sky and the chosen redshift range, but for concreteness we will assume that most extragalactic work will explore a range of redshifts from $z = 0$ to $z = 4$, which encompasses most of the star-formation history of the universe. For such surveys, areas on the order of 1 deg^2 are needed in order to maintain fractional errors on number counts near the 10% level and to probe a wide range of cosmic structures. This is fairly easy to demonstrate using online tools such as the Cosmic Variance Calculator[11] described in Trenti & Stiavelli (2008), but an even simpler way to show this is to use the analytic expressions provided by Driver & Robotham (2010) to estimate and compare cosmic variance for different field sizes. These authors employed counts of galaxies near the characteristic break in the luminosity function (M^*) in the Sloan Digital Sky Survey Data Release 7 (SDSS DR7; Abazajian et al. 2009) to derive an empirical expression connecting cosmic variance and survey volume. Assuming a single sight line and a rectangular geometry, the fractional error in the counts of M^* galaxies is given by:

$$
\begin{aligned}
\zeta = &(1 - 0.03(\sqrt{(A/B) - 1}) \\
&\times (219.7 - 52.4(\log_{10}[A \cdot B \cdot 291.0]) \\
&+ 3.21(\log_{10}[A \cdot B \cdot 291.0]^2))\sqrt{C/291.0}.
\end{aligned} \tag{1}
$$

where A, B, and C are the median redshift transverse lengths and the radial depth of the survey, respectively, expressed in units of $h_{0.7}^{-1}$ Mpc. (Note that the derived cosmic variance is for $M^* \pm 1$ mag population only and will take higher values for more massive halos; see, e.g., Moustakas & Somervillle 2002.) Results computed using this equation are presented in Figure 2, which shows the calculated cosmic variance for a number of surveys and compares these with our proposed field size of around 1 deg^2 (actually $55' \times 55'$, for technical reasons described subsequently).

Figure 2 shows that the calculated cosmic variance for our proposed field size results in fractional counting errors of around 10–15% (per unit redshift interval) for counts of M^*

---

[11] See http://casa.colorado.edu/~trenti/CosmicVariance.html.
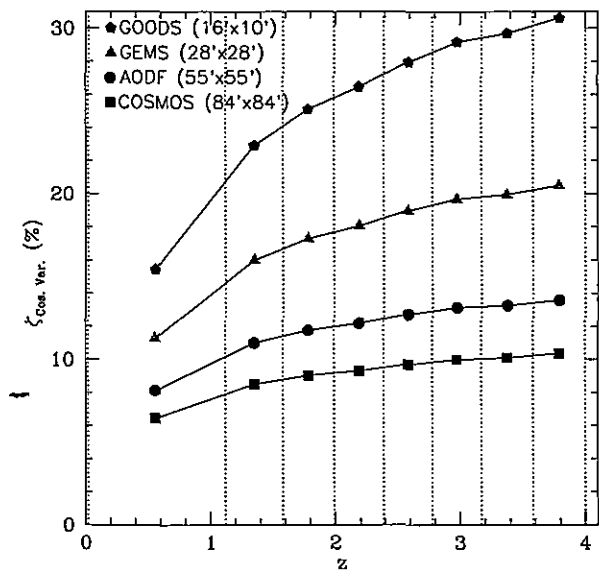
FIG. 2.—Cosmic variance, quantified using eq. (1), as a function of redshift for four fields covering different areas on the sky. Redshifts of presented points correspond to median values for redshift ranges indicated with dotted lines. The effect of small-scale inhomogeneity on the field size we propose (~ 1 deg^2, denoted as AODF) is comparable with the COSMOS field cosmic variance and much less prominent than in the other two (smaller) fields, GEMS and GOODS. See the electronic edition of the *PASP* for a color version of this figure.

galaxies at redshifts between $z = 1$ and $z = 4$. This is only slightly higher than for the COSMOS field (Scoville et al. 2007), but quite significantly better than for smaller-volume survey fields, such as Galaxy Evolution from Morphology and SEDs (GEMS; Rix et al. 2004) and Great Observatories Origins Deep Survey (GOODS; Dickinson et al. 2003). On this basis alone we would argue that something around 1 deg^2 is probably the right minimum size for a contiguous area survey field intended to allow a broad range of investigations using adaptive optics, although another important factor is that a survey of this size will contain many thousands of strong line-emitting objects, which are obvious targets for present-generation AO systems.

We have computed the surface density of strong H_α line emitters (which we define to be $F_{H_\alpha} > 10^{-16}$ ergs cm^2 s^{-1}, corresponding to the flux density of bright line emitters in (Förster-Schreiber et al. (2009); Law et al. (2009) on the basis of direct measurement (Villar et al. 2008; Shim et al. 2009), as well as using indirect estimates scaled from UV flux (Bouwens et al. 2009) and measurements of [O II] (Cooper et al. 2008). By incorporating all the available information, we estimate this value to be 2–5 H_α line emitters with flux $>10^{-16}$ ergs cm^2 s^{-1} Å^{-1} arcmin^{-2} at $1 < z < 1.5$, declining to 1–2 arcmin^{-2} in the redshift interval $2 < z < 2.5$. The deep fields proposed in this article will thus have around 10,000 suitable targets

for AO-based follow-up. A significant fraction of these will be lost for various reasons (e.g., if H_α lies on an airglow emission line; Davies et al. 2008), and a small number of remaining objects will still lack suitable guide stars (see § 5). However, thousands of AO-accessible targets will remain, presenting a multiple-order-of-magnitude change from the current situation.

2.3. Guide Star Limitations

We now explore the brightness of natural guide stars needed for effective use of adaptive optics. Our focus will be on the following three classes of AO systems:

Case 1.—Laser-assisted adaptive optics systems on 8 m class telescopes, for which natural guide stars are needed to supply tip-tilt corrections. Such systems will define the state of the art for the next few years.

Case 2.—Ground-layer adaptive optics systems for 4 m class telescopes. Such systems are now being proposed as a means of revitalizing 4 m class facilities (e.g., Canada-France-Hawaii Telescope [CFHT] 'IMAKA; Lai et al. 2008). These facilities will also require natural guide stars for tip-tilt correction.

Case 3.—AO systems on 30 m class telescopes, some designs for which rely on AO for routine operation. In this case we mainly seek fields with an abundance of natural guide stars bright enough to feed laser-*unassisted* AO systems. Laser beacons may not be available at all times, and the existence of extragalactic fields in which they are not essential may be extremely attractive for telescopes that heavily emphasize AO.

We will begin by first outlining the general problem before focusing on the parameter space appropriate to the specific preceding cases. As will be shown subsequently, in practice, it is cases 2 and 3 that drive our chosen magnitude limits.

In order to function an AO system needs to capture photons from a star, compute a correction, and apply this correction to an optical surface. The frequency over which an AO system must operate is set by the velocity of the atmosphere and the atmospheric coherence length. The coherence length is the length scale over which the index of refraction of the atmosphere is effectively constant and is typically around 10 cm at a good site. Wind speeds in the upper atmosphere are around 20 m/s, so it typically takes around 0.005 s for a patch of atmosphere to move a coherence length (Rogemann & Welsh 1996). The minimum frequency of an AO system is therefore around 200 Hz, although, in reality, one would want to both Nyquist-sample the signal and allow time for actuator lag in applying a correction, so a realistic minimum is around 1 kHz.

How many photons from a natural guide star are needed in this time depends on the specific type of correction, but we can bracket our analysis by considering two extremes: (1) tip-tilt correction, for which relatively faint stars suffice, and (2) full correction to obtain diffraction-limited performance, for which bright stars are needed.

A zeroth magnitude star has a R-band flux of 3080 Jy at the top of the atmosphere,[12] corresponding to 2.02×10^{11} photons m^{-2} s^{-1} (Bessell 1979). Thus, an 8 m telescope captures ~600 R-band photons from an 18th magnitude star in 1 ms. In the foreseeable future no AO system will have a quantum efficiency approaching unity, but even with an end-to-end efficiency of 20%, over 100 photons will remain, which is ample for obtaining a reasonable centroid. Thus, at least in principle, an AO system on an 8 m telescope can use $R = 18$ mag stars for tip-tilt corrections. Since the number of photons from a star imaged with a 30 m telescope is about 14 times greater than for an 8 m telescope, a 30 m telescope can do tip-tilt corrections on guide stars down to around $R = 21$ mag. On the other hand, a 4 m telescope needs stars of about $R = 16.5$ mag for tip-tilt corrections. We emphasize that these numbers are all for rather idealized AO systems. For example, in the real-world situation of the Gemini Altair AO system, tip-tilt reference stars of around $R \sim 16.5$ mag (over a magnitude brighter than the somewhat ideal case discussed previously) are found to be highly desirable for high-performance AO operation.

Much brighter natural guide stars are needed for use with natural guide AO star systems that attempt to achieve diffraction-limited performance. In this case the size of relevance is not the full aperture of the telescope, but rather the subaperture defined by the coherence length of the atmosphere, which in turn drives the number of needed actuators. An $R = 13$ mag star supplies ~10 photons in 1 ms to a 10 cm diameter subaperture. The number of photons per bin needed to reliably compute a wavefront depends critically on factors such as the read noise of the detector, but 10 photons per coherence-length-sized patch on the pupil is a reasonable lower limit. Note that in the case of diffraction-limited AO (and unlike the case with tip-tilt correction), having a larger telescope does not gain one a fainter magnitude limit for natural guide stars; in fact, AO becomes harder, because the system requires more actuators. We also note that the presence of bright stars ($R \lesssim 14$ mag) in the field with AO correction can potentially cause problem for infrared (IR) detectors by leaving long-lasting (up to 1 hr) residual flux. Although this would affect imaging in the case when AO correction is applied across a wide field of view, the main motives for developing an AO-friendly deep field (see §§ 1 and 5) are high-resolution IFU or multiobject spectroscopic surveys, which would not be influenced.

On the basis of the considerations just given, our search for locations on the sky suitable for extragalactic adaptive optics focuses on stars in the magnitude range $13 < R < 16.5$ mag. The bright end is set by the apparent magnitude of stars needed to supply guide stars for NGS AO systems (independent of telescope aperture), which is essentially case 3. The faint end is set by the apparent magnitude of stars needed to supply tip-tilt

reference stars for real-world operation of existing AO systems on 8 m class telescopes (case 1) and for ideal-case laser-based ground-layer AO with 4 m class telescopes (case 2).

3. IDENTIFICATION OF THE SUITABLE FIELDS FOR ADAPTIVE OPTICS

In order to find the regions on the sky with the properties we have just described, we rely on full-sky reprocessed composites of the *COBE*/DIRBE and IRAC/ISSA dust maps (Schlegel et al. 1998) and the UCAC2 astrometric catalog of ~5 × 10^7 stars with declination in the $[-90°, +(40–52)°]$ range (Zacharias et al. 2004). We constructed a full-sky map of star-count surface density for UCAC2 stars in the range 13–16.5 mag using the HEALPix data analysis package (Górski et al. 2005) that performs pixelization of the sphere with equal-area pixels. Two maps have been produced: one with the resolution of 6.871′ to match the resolution of the available HEALPix map of Galactic reddening $E(B - V)$ and the other (see Fig. 3) with the coarser sampling of 55′ (the HEALPix resolution that is closest to the 1° × 1° field size, see § 2.2). The resolution of the existing $E(B - V)$ map was degraded to match the 55′ resolution of the star-count surface density map by taking the average extinction value for each cell. The coarse resolution extinction and star-count maps are both shown as panels at the top left and top right of Figure 3. Note that the UCAC2 catalog has a gap in coverage at high declination (shown in gray in the figure), but any AO-optimized fields that might exist at these very high declinations would be generally unsuitable anyway. Any such fields would be inaccessible from Chile and be at quite high air mass most of the time for major northern hemisphere observatories (including those on Mauna Kea).

Before proceeding with a detailed analysis, it is instructive to note that many positions in the sky likely to be suitable for our purposes can be identified easily by simply looking for maxima in a map obtained by multiplying the stellar density map by the inverse of the extinction map. This is shown as the large bottom panel in Figure 3. Local maxima in this map do not necessarily define regions suitable for AO, because some local maxima correspond to regions with low star counts but extremely low extinction. However, this figure acts as a natural starting point for the next step in our analysis.

Having identified candidate fields using the analysis just described, we then looked at all the candidate fields individually to try to better understand their characteristics. To be explicit, we first identified all HEALPix cells whose $13 < R < 16.5$ mag stellar density Σ_{sc} was $\Sigma_{sc} > 0.5$ arcmin^{-2} and whose extinction was $E(B - V) \lesssim 0.1$. We found 442 1 deg^2 cells met these criteria, and these were then examined further. The distribution of stellar density and extinction for these cells is shown in Figure 4, shaded by right ascension. In order to cull these fields down to a more manageable number, we then restricted the sample further to include only those fields whose extinction is lower than the average extinction and whose stellar density is higher

---

[12] For concreteness we consider the brightness of guide stars at visible wavelengths, though the argument can be generalized to stars at arbitrary wavelength.
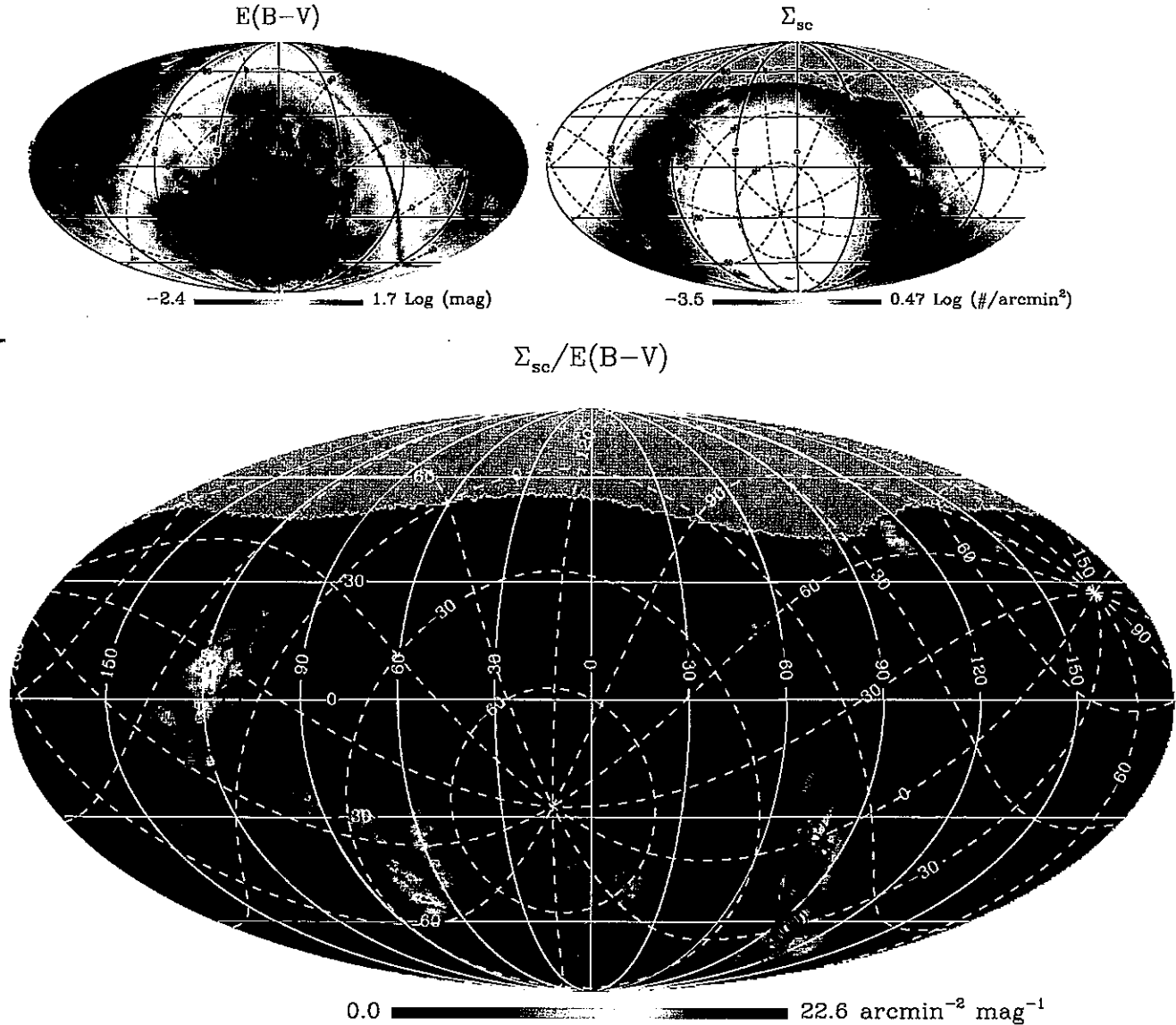
E(B−V)

Σ_{sc}

−2.4 ▆▆▆▆▆▆▆▆▆▆▆▆▆▆ 1.7 Log (mag)

−3.5 ▆▆▆▆▆▆▆▆▆▆▆▆ 0.47 Log (#/arcmin²)

Σ_{sc}/E(B−V)

0.0 ▆▆▆▆▆▆▆▆▆▆▆▆▆▆▆▆ 22.6 arcmin^{-2} mag^{-1}

FIG. 3.—*Top left*: An all-sky map of extinction, scaled logarithmically. The solid-line grid corresponds to the celestial coordinate system with right ascension in degrees increasing to the left. Zero degrees lies at the center of the figure. A Galactic coordinate system is overplotted with dashed lines. *Top right*: The corresponding map of star-count surface density for stars in the 13–16.5 mag range. The region shown in gray corresponds to a high-declination gap in coverage in the UCAC2 stellar catalog. As noted in the text, any AO-friendly fields that might exist at very high declination would be unsuitable for other reasons. *Bottom*: A map constructed by multiplying the map at the top left by the inverse of the map at the top right. Maxima in this figure correspond to potentially interesting locations for undertaking extragalactic adaptive optics observations. Circles present the positions of 67 fields that are well suited to extragalactic AO. See the text for details. See the electronic edition of the *PASP* for a color version of this figure.

than the average density. This translates into selecting fields with a stellar density greater than 0.65 arcmin^{-2} and reddening less than ~0.087 mag. This final cut corresponds to selecting fields inside the dashed region shown in Figure 4 and brings the total number of fields down to 67 from 442. The positions of these fields are shown as solid dots in Figure 3 and squares in Figure 1.

The locations and properties of the 67 fields are given in Table 1. Variances and higher-order moments of stellar counts and extinction within each field are also tabulated. These moments are based on computations within subcells with widths of 6.871′. The fields flagged with open circles in Figure 4 have the highest star-count surface density or the lowest average value or standard deviation of the reddening coefficient, and rows corresponding to these fields are italicized in the table. Shaded arrows point at some more representative fields for the three sight lines (see Appendix A for details). A graphical summary of all higher-order statistics is presented in Figure 5,
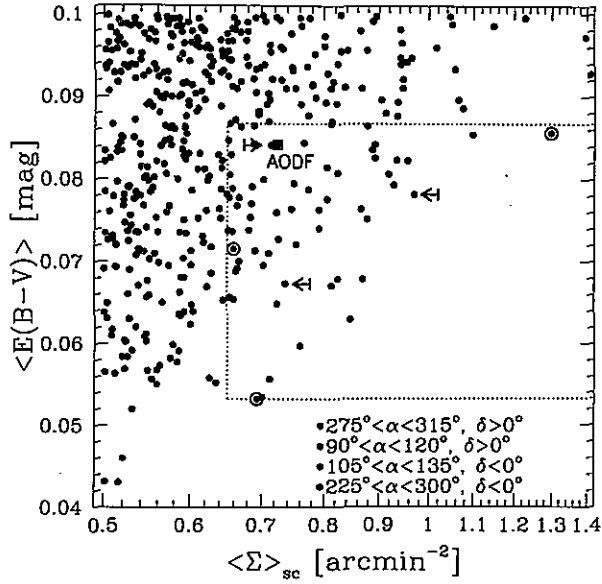
FIG. 4.—Extinction $E(B-V)$ as a function of the star-count surface density Σ_{sc} for 442 $55' \times 55'$ fields with $\Sigma_{sc} > 0.5$ arcmin^{-2} and $E(B-V) \lesssim 0.1$. The fields are shaded based on their equatorial coordinates. The dashed line encloses 67 fields with $\Sigma_{sc} \geq 0.65$ arcmin^{-2} and $0.05 \lesssim E(B-V)$[mag] $\lesssim 0.087$. The fields flagged with open circles have the highest star-count surface density or the lowest mean extinction or its standard deviation. Shaded arrows point at the representative fields for each of the three sight lines (see Appendix A for details). The proposed optimal field described in § 4 is labeled AODF and flagged with an open box. See the electronic edition of the *PASP* for a color version of this figure.
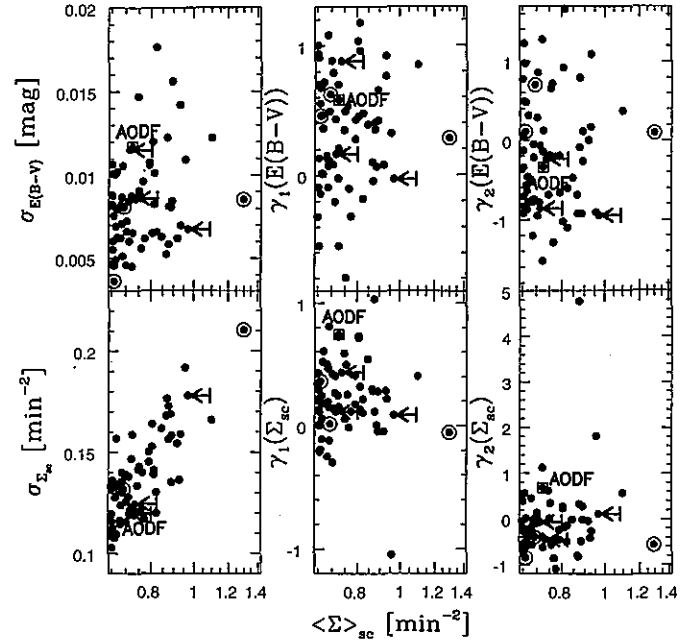

FIG. 5.—Three higher-order moments of the extinction and star-count surface density distributions as functions of the mean star-count surface density for 67 fields from Table 1. The fields are shaded based on their equatorial coordinates, as given in Fig. 4. The fields flagged with open circles or with shaded arrows correspond to the flagged fields in Fig. 4. Our optimal AO-friendly field is labeled as in Fig. 4. See the electronic edition of the *PASP* for a color version of this figure.

from which it can be seen that there is a substantial variation in the distribution of both stars and extinction throughout the fields we have identified. While all the tabulated fields should be quite good for extragalactic adaptive optics work, the best field for a given purpose will depend upon the specific application (e.g., upon whether it is more important to maximize uniformity of star counts, or to minimize absolute extinction, or to minimize variation in extinction). The various tradeoffs that need to be balanced in order to choose the best field for a given set of requirements are explored in Appendix A.

4. CFHT IMAGING RESULTS FOR A PROPOSED OPTIMAL FIELD

All fields labeled in Figure 1 and in the lower panel of Figure 3 have exceptional characteristics in terms of stellar surface density and/or extinction.[13] However, a practical factor that has

---

[13] It is interesting to speculate on why these fields exist. While many of them lie in the vicinity of Badde's Window, characterized by very low dust content, a smaller group of fields is found near the Galactic anticenter. One possibility (S. van den Bergh 2010, private communication), is that these fields have high counts but low extinction, because metallicity decreases with increasing galactocentric distance. As a result, the Galactic anticenter has a low dust-to-gas ratio.

not yet been considered is the position of the field for accessibility with a broad range of telescopes. An ideal field lies near zero degrees declination in order to be reachable from both hemispheres. With this consideration in mind, the most interesting region for further analysis proves to be the rather large $30° \times 60°$ region centered at R.A. $= 8^h$, decl. $= 0°$ (see the bottom map in Fig. 3). To identify the best 1 deg^2 patch within this region, we tessellated the region into $55' \times 55'$ cells and explored the distribution of star counts and $E(B-V)$ on a cell-by-cell basis. After identifying a handful of promising cells, we then looked for both low absolute extinction and uniformity in extinction within individual cells. (Uniformity in extinction is desirable for accurate photometric redshifts). Figure 6 shows the intracell stellar surface density and the extinction map for the best $55' \times 55'$ cell, which we refer to as the adaptive optics deep field (AODF). The field lies at R.A.: $7^h24^m3^s$, decl.: $-1°27'15''$ and is labeled (in bold) with ID 8328 in Table 1. It has a stellar surface density of more than two stars per $2' \times 2'$ region over >99% of its area. In addition, for >85% of the field presented in Figure 6 extinction is $E(B-V) \lesssim 0.1$ ($A_V < 0.3$; NIR extinction at AO wavelengths will be far lower; see § 2). Another important practical consideration is that the number of very bright stars (which scatter and raise the sky background) in this ~1 deg^2 field is low: there are only a handful of stars brighter than 11th magnitude in the field.
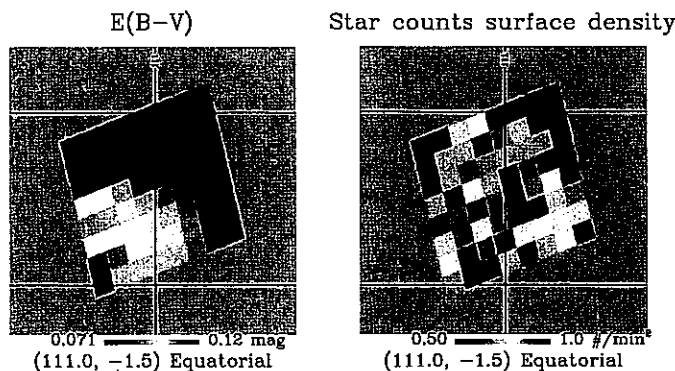
E(B−V) Star counts surface density

0.071 ▬▬ ▬ 0.12 mag   0.50 ▬▬ ▬ 1.0 #/min²
(111.0, −1.5) Equatorial (111.0, −1.5) Equatorial

FIG. 6.—Extinction and star surface density maps centered on the position of our chosen field. Each pixel is 6.871″ × 6.871″. There are ≳2200 13–16.5 mag stars suitable for AO guiding in the field corresponding to ~3300 star-forming galaxy candidates with the number surface density of 3 arcmin⁻². The field is centered at R.A. = $7^h24^m2.67^s$, decl. = −1°27′14.44″. The solid-line grid corresponds to the celestial coordinate system with R.A. [°] = 360° − α [°]. See the electronic edition of the *PASP* for a color version of this figure.

Since this AODF field seems highly interesting for future follow-up, Director's Discretionary time on the CFHT was used to explore its properties further (and to act as a sanity check on the analysis presented in this article). A 10 minute snapshot in g' and z' bands was acquired using CFHT's MegaCam in 2010 March in order to evaluate the distribution and color of the brightest stars in the AODF (see Bertin et al. 2002 for the description of the TeraPIX software modules designed for processing MegaCam data). The upper panel of Figure 7 presents the ~1° × 1° field of view (made out of five dithered exposures), and it is apparent here that bright stars are indeed sparse, with the most prominent one ($V = 9.9$ mag) in the center of the field. The main drawback of such a star is not the vertical blooming, which affects a small fraction of the imaging area, but the halos due to internal reflections in the MegaPrime optics: such a halo locally increases the sky background and limits detectivity. The upper panel of Figure 7 shows that there are four stars that cause a potential problem. Each halo covers a disk of 3′ in radius, leading to ~120 arcmin² for the whole field. When compared with the MegaCam field of view of ~1 deg², those four halos produce a negligible loss of less than 4%. (We note that brighter galaxies can still be extracted from these areas.)

We also compared AODF galaxy counts in g' and z' bands with the expected number based on the CFHT Legacy Survey (CFHTLS) Deep data (details on galaxy/star separation method used by the TeraPIX pipeline are given in Coupon et al. 2009). The resulting depth found in both g' and z' bands follow the expectations (within the range of error), and the recovered galaxy number surface density closely tracks the distribution of CFHTLS Deep objects, as shown in the lower panel of Figure 7. The slight excess at the bright end is the combined effect of shot noise and cosmic variance (see § 2.2), and the turnover at $g = 24.5$ mag is due to the (much) shorter exposure time, compared with the CFHTLS Deep.

We conclude from analysis of the CFHT data that all the characteristics discussed in this section (namely, a position that

allows observations from different sites, a large number of suitable tip-tilt stars for laser AO, a generally low and fairly uniform Galactic extinction, coupled with the small number of very bright stars) make this particular field an excellent choice for future deep extragalactic AO observations.

5. REAL-WORLD BENEFITS OF UNDERTAKING OBSERVATIONS IN AO-OPTIMIZED FIELDS

How do the properties of the fields identified in the previous sections compare with those of existing extragalactic deep fields? Figure 8 presents a comparison of the average stellar density, average extinction, and standard deviation of the extinction coefficient for the set of 67 55′ × 55′ fields from Table 1 to those in 55 existing deep fields.[14] Quantities are shown as functions of Galactic latitude, with our candidate fields shown as filled circles at low Galactic latitudes' and existing deep fields shown as filled circles at high Galactic latitudes. Our preferred field is labeled F in each panel. The figure illustrates that our proposed fields typically have over 10 times the stellar density of existing deep fields coupled with extinction values and extinction variations across the field at the high end of those in existing deep fields.[15] How does this translate into practical performance benefits for undertaking AO observations? Are the existing fields already good enough? In order to investigate these questions, we will define a fairly generic figure of merit for AO observations in § 5.1 and compare the distribution of this figure of merit in our proposed fields with the corresponding distribution in a typical existing deep field (§ 5.2).

---

[14]From the list compiled by J. Brinchmann; see http://www.strw.leidenuniv.nl/~jarle/Surveys/DeepFields/index.html.

[15]Note that in Fig. 8 we have also included a region within the CFHTLS W2. This is not technically a deep field, but CFHTLS W2 is worthy of inclusion because it is the most commonly observed extragalactic field that lies in the general vicinity of our preferred field (for detailed descriptions and comparisons with this field, see § 5.2).

FIG. 7.—*Top:* CFHT MegaCam g'- and z'-band mosaic of the $1° \times 1°$ field centered on R.A. $= 7^h24^m$, decl. $= -1°27'15''$. Note that there are only a few bright stars in this field, with the brightest one (in the middle of the field) at $V = 9.9$ mag. *Bottom:* Galaxy number per 0.5 mag and per $1° \times 1°$ as a function of g' magnitude. The solid line represents the expected values based on CFHTLS Deep data set and triangles correspond to the recovered galaxy number counts. See the electronic edition of the *PASP* for a color version of this figure.

FIG. 8.—*Top left:* Stellar surface density as a function of Galactic latitude for two sets of deep fields: 55 existing deep fields plus 1 deg^2 region within the CFHTLS W2 field (*filled circles at high Galactic latitudes*) and 67 low-latitude pointings we have explored in detail (*filled circles at low Galactic latitudes* [detailed properties listed in Table 1]). *Top right:* Average $E(B - V)$ as a function of Galactic latitude for the same two sets of fields. *Bottom right:* Standard deviation of $E(B - V)$ for the data in the other panels (this panel quantifies the patchiness of the extinction). Our chosen field (AODF) and five other fields from Table 1 with extreme properties are labeled. See the electronic edition of the *PASP* for a color version of this figure.

Optics System (Gemini MCAO, Ellerbroek et al. 2003). Gemini MCAO is intended to feed NIR instruments with a high Strehl ratio beam at relatively short wavelengths (Strehl ratios up to ~50% in the J band) and, in particular, to feed the Florida Multi-Object Imaging Near-Infrared Grism Observational Spectrometer (FLAMINGOS-2) NIR MOS spectrograph (Eikenberry et al. 2004) and the Gemini South Adaptive Optics Imager (GSAOI) imaging camera (McGregor et al. 2004). The benefits of undertaking observations in the AODF are fairly obvious for science programs that use imaging cameras or resolved integral-field spectrographs, but the AODF will also be of considerable interest for programs of NIR MOS spectroscopy. Some spatially resolved kinematical and chemical composition information can be recovered with narrow slits if these span individual objects that are not obliterated by seeing. Furthermore, AO-assisted MOS spectrographs will be able to effectively use narrow slits, which minimize background contamination.

We have chosen to focus our analysis on Gemini MCAO because it is the most advanced AO system likely to be available on 8 m class telescopes for the foreseeable future and because MCAO is virtually certain to be an important operational mode for future 30 m class ELTs. We will not describe the fundamentals of MCAO here, and we refer the reader to Rigaut et al.

For the sake of concreteness, much of the following analysis will be undertaken in the context of the predicted performance of the soon-to-be-commissioned Gemini Multiconjugate Adaptive
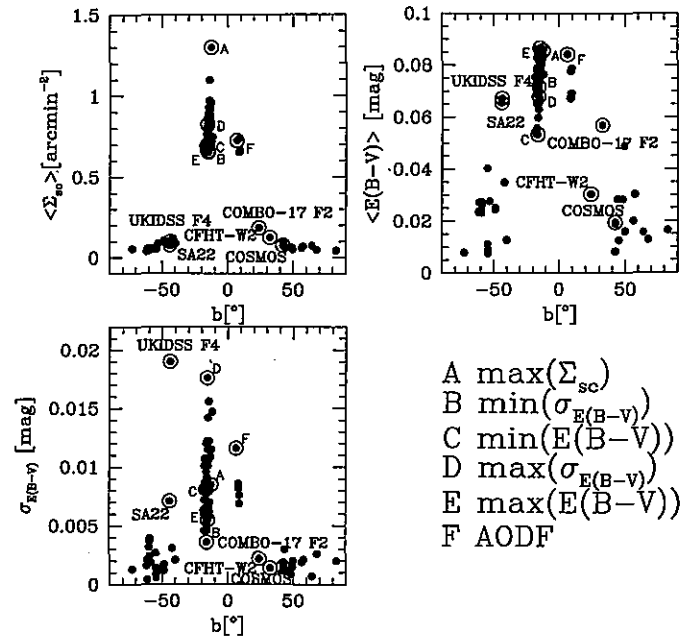
TABLE 1
PROPERTIES OF THE $55' \times 55'$ FIELDS IDENTIFIED IN FIGS. 3 AND 4

No.[a]	α (h m s)	δ (° ′ ″)	Σ_{SC} (min^{-2})	$\delta\Sigma_{SC}$ (min^{-2})	$\gamma_1(\Sigma_{SC})$[b]	$\gamma_2(\Sigma_{SC})$[c]	$E(B-V)$ (mag)	$\delta_{E(B-V)}$ (mag)	$\gamma_1(E(B-V))$[d]	$\gamma_2(E(B-V))$[e]
8273	08 01 55.8886	−14 35 51.1368	0.6529	0.1159	0.2201	−0.1935	0.0778	0.0082	0.6996	−0.3415
8276	08 05 33.3355	−14 52 48.6047	0.6648	0.1331	0.0565	−0.2372	0.0692	0.0069	0.4663	−0.6372
8328	**07 24 02.6662**	**−01 27 14.4438**	**0.7243**	**0.1199**	**0.7418**	**0.6834**	**0.0842**	**0.0116**	**0.5841**	**−0.3379**
16758	19 26 57.2356	−21 00 06.8527	0.6512	0.1322	0.4283	0.5339	0.0847	0.0046	−0.0902	−0.1311
16759	19 25 39.0129	−20 08 11.7480	0.6886	0.1399	0.1533	−0.1122	0.0865	0.0051	0.1163	−0.2162
16760	19 26 03.2858	−23 06 02.0956	0.6552	0.1361	0.1152	−0.6959	0.0830	0.0060	0.9076	1.2258
16807	19 13 28.5182	−33 29 53.6142	0.6836	0.1144	−0.2496	−0.1904	0.0754	0.0082	0.1264	−0.7768
16813	19 09 30.5475	−33 53 54.2514	0.6698	0.1095	0.6056	−0.2252	0.0864	0.0063	0.7165	0.3145
17007	18 45 32.0045	−44 18 15.3369	0.6625	0.1077	0.2454	0.0127	0.0689	0.0101	0.6913	−0.5662
17013	18 51 34.5808	−39 41 51.5158	0.6859	0.1354	0.4643	−0.2977	0.0791	0.0087	0.0751	−1.2020
17016	18 48 11.6290	−43 03 10.6952	0.6493	0.1335	0.3393	−0.0503	0.0782	0.0082	−0.3202	0.7728
17018	18 43 39.3947	−43 27 05.7019	0.6668	0.1345	0.5197	−0.5390	0.0778	0.0079	0.0102	−0.8005
17019	18 41 51.8111	−42 35 40.4388	0.8053	0.1637	0.7161	0.2299	0.0776	0.0120	0.4575	−1.0243
17020	18 44 35.3906	−41 20 37.7884	0.7226	0.1468	0.7250	1.1223	0.0843	0.0088	0.6999	1.2784
17021	18 42 54.1928	−40 28 59.3417	0.8050	0.1526	0.7322	0.2712	0.0815	0.0065	1.0337	0.9215
17022	18 40 08.9584	−41 44 00.6738	0.8661	0.1679	0.2980	−0.7967	0.0764	0.0052	0.1027	−0.6874
17023	18 38 30.5484	−40 52 07.4231	0.8916	0.1350	−0.0433	0.2787	0.0826	0.0084	0.6570	−0.2598
17075	18 27 58.8002	−51 47 48.6539	0.6516	0.1194	0.2052	0.3915	0.0738	0.0107	1.0010	0.0506
17077	18 29 04.8143	−49 41 42.1637	0.6572	0.1124	0.0020	−0.2874	0.0737	0.0046	0.5543	0.9716
17078	18 25 53.1372	−50 56 23.1299	0.7260	0.1587	0.1519	−0.6180	0.0728	0.0065	−0.5469	0.1232
17079	18 23 54.2239	−50 04 40.8792	0.7656	0.1402	−0.0137	−0.8646	0.0845	0.0096	−0.1007	−1.2872
17091	18 40 01.0208	−46 48 19.8550	0.7031	0.1157	0.1433	−0.0895	0.0696	0.0072	0.7903	0.8552
17093	18 40 53.8719	−44 42 07.6520	0.6906	0.1311	−0.1203	−0.3673	0.0713	0.0081	0.4937	−0.7466
17094	18 38 04.1331	−45 57 7.0615	0.6536	0.1029	0.1297	−0.5615	0.0657	0.0101	0.1336	−0.9206
17095	18 36 12.7661	−45 05 38.2141	0.7593	0.1210	0.2531	−0.5653	0.0598	0.0056	0.5337	0.7193
17096	18 37 08.7827	−48 03 18.3032	0.7012	0.1389	0.4229	0.08	0.0535	0.0046	0.8826	0.2867
17097	18 35 09.7115	−47 12 03.1888	0.7124	0.1380	0.4046	−0.0505	0.0557	0.0060	0.4347	−0.0656
17098	18 32 10.1262	−48 26 55.1962	0.7240	0.1214	0.1241	−0.4096	0.0649	0.0045	0.2076	−0.1427
17099	*18 30 14.9620*	*−47 35 20.7596*	*0.6929*	*0.1318*	*0.0147*	*−0.3991*	*0.0533*	*0.0081*	*0.6250*	*0.7012*
17100	18 33 16.4493	−46 20 31.8008	0.7921	0.1450	0.1766	−0.4501	0.0741	0.0107	0.4304	−0.6588
17101	18 31 28.6253	−45 28 45.3891	0.8453	0.1615	0.5415	−0.0136	0.0630	0.0063	0.3935	−0.4720
17102	18 28 25.4970	−46 43 31.1481	0.8691	0.1763	0.2818	−0.8206	0.0679	0.0122	−0.0426	−0.9224
17103	18 26 41.3603	−45 51 27.5153	0.7914	0.1501	0.4085	−0.2372	0.0764	0.0106	0.2804	−0.1952
17104	18 39 4.4069	−43 50 40.8234	0.7537	0.1431	0.4959	0.3473	0.0722	0.0088	−0.7946	0.6602
17105	18 37 19.8926	−42 58 59.3005	0.7498	0.1416	0.0553	0.0113	0.0795	0.0091	0.4961	−0.1894
17106	18 34 26.5970	−44 13 54.4803	0.8241	0.1198	0.1038	−0.1377	0.0679	0.0176	0.4784	−1.1006
17107	18 32 45.2756	−43 21 56.9586	0.8132	0.1411	0.1348	−0.1838	0.0671	0.0101	0.9592	1.6666
17108	18 35 40.0269	−42 07 04.1409	0.8770	0.1726	0.1150	0.3291	0.0752	0.0081	0.4070	−0.0853
17109	18 34 04.5145	−41 14 56.3333	0.8866	0.1687	0.0054	−0.4840	0.0836	0.0080	0.0681	−0.9237
17110	18 31 08.5135	−42 29 46.6791	0.8916	0.1581	0.2791	−0.0116	0.0843	0.0156	0.4232	0.1181
17112	18 29 45.8757	−44 36 45.0522	0.9283	0.1362	0.2869	−0.4116	0.0794	0.0142	0.7674	0.1725
17114	18 25 02.1950	−44 59 10.9323	0.9693	0.1778	0.0847	0.1121	0.0782	0.0067	−0.0307	−0.9453
17115	18 23 27.6851	−44 06 42.3880	0.9336	0.1587	0.2213	−0.2587	0.0824	0.0070	0.9227	1.0957
17116	18 26 34.3634	−42 52 06.7502	0.9180	0.1542	−0.0436	−0.0388	0.0807	0.0062	0.0834	0.0063
17118	18 21 57.5217	−43 14 2.7750	0.9554	0.1916	−1.0498	1.8245	0.0823	0.0109	0.3205	−0.9074
17120	18 27 07.7550	−48 50 04.1290	0.6671	0.1567	0.1793	−0.4337	0.0701	0.0102	0.3642	−0.4607
17121	18 25 16.6832	−47 58 10.7959	0.7111	0.1280	0.2671	−0.0459	0.0710	0.0084	−0.2037	−0.7853

TABLE 1 (Continued)

No.[a]	α (h m s)	δ (° ' ")	Σ_{SC} (min^{-2})	$\delta\Sigma_{SC}$ (min^{-2})	$\gamma_1(\Sigma_{SC})$[b]	$\gamma_2(\Sigma_{SC})$[c]	$E(B-V)$ (mag)	$\delta_{E(B-V)}$ (mag)	$\gamma_1(E(B-V))$[d]	$\gamma_2(E(B-V))$[e]
17177	18 50 24.7353	−33 44 49.6317	1.0975	0.1658	0.4016	0.5773	0.0855	0.0122	0.8477	0.3780
17188	18 46 40.5524	−37 07 1.4218	0.8116	0.1389	0.3189	−0.1815	0.0867	0.0083	1.1766	1.7831
17288	18 23 39.5297	−41 06 44.2969	1.2965	0.2105	−0.0562	−0.5628	0.0857	0.0085	0.2818	0.0993
18560	17 30 4.4220	−59 55 39.3082	0.8774	0.1563	1.0359	4.7730	0.0865	0.0058	0.3543	0.7979
22659	20 34 1.8777	+18 41 40.5432	0.7140	0.1193	0.1133	−0.0646	0.0842	0.0115	0.1667	−0.8588
22665	20 30 15.9096	+18 28 26.4926	0.7461	0.1334	0.5894	0.6151	0.0764	0.0147	0.3505	−0.6854
31486	08 04 54.9932	−15 47 16.2648	0.7365	0.1243	0.4348	−0.4508	0.0674	0.0086	0.8794	−0.2353
31487	08 08 34.1773	−16 03 51.0974	0.6575	0.1107	−0.2133	0.5630	0.0789	0.0076	−0.1390	−0.8436
48510	17 40 30.1826	−61 25 54.5380	0.6592	0.1329	0.3597	−0.8497	0.0716	0.0036	0.4596	0.1084
48511	17 38 41.6103	−60 32 25.4590	0.7031	0.1256	−0.2966	0.1368	0.08	0.0066	0.0875	−0.9509
48593	17 34 57.5166	−62 37 9.1809	0.6595	0.1102	−0.1926	−0.5202	0.0654	0.0046	0.6758	0.4808
48594	17 29 01.5184	−63 47 46.8549	0.6850	0.1238	0.1940	−0.5662	0.0771	0.0071	−0.0907	−0.5278
48595	17 27 18.9816	−62 53 54.7870	0.7736	0.1170	0.1161	−1.0970	0.0788	0.0062	−0.3162	−0.2015
48596	17 33 11.4505	−61 43 28.8547	0.7230	0.1231	0.2457	−0.3871	0.0760	0.0115	−0.0218	−1.5210
48597	17 31 34.0292	−60 49 38.5446	0.8235	0.1301	0.2149	−0.4993	0.0808	0.0066	−0.1810	−0.6031
48600	17 21 01.3747	−64 03 37.7765	0.6813	0.1162	0.5003	0.4488	0.0739	0.0062	0.1536	−0.7576
48610	17 00 14.0968	−68 21 58.8538	0.6641	0.1276	−0.1090	−0.6135	0.0768	0.0049	0.0170	−0.8740
48611	16 59 02.2874	−67 27 18.9130	0.6539	0.1090	0.0080	−0.6701	0.0868	0.0055	−0.5483	−0.7081
48915	16 19 26.1713	−71 39 37.6062	0.6536	0.1084	0.2919	−0.7719	0.0806	0.0088	0.9343	0.4950
48918	16 19 40.9547	−70 44 32.6440	0.6883	0.1352	0.8101	−0.0178	0.0843	0.0106	1.0809	−0.0507

[a] Pixel number based on $N_{side} = 64$ HEALPix partition of the sphere.
[b] Third moment of distribution (skewness) for star-count surface density.
[c] Fourth moment of distribution (kurtosis) for star-count surface density.
[d] Third moment of distribution (skewness) for extinction.
[e] Fourth moment of distribution (kurtosis) for extinction.

(2000) for an explanation of the general principles. For our purposes it suffices to note that MCAO's purpose is to deliver high image quality over a wider area than conventional adaptive optics systems, and it does so by using a constellation of laser guide stars beacons and several natural guide stars to determine the shape of the wavefront, which is then corrected by multiple deformable mirrors. (The natural guide stars are essential, because they are needed in order to establish tip-tilt corrections.) In the case of the Gemini MCAO system, five artificial guide star beacons and three natural guide stars are used. Another important point that should be emphasized here is that the precision of the tip-tilt corrections depends on distance from the guide stars, so the geometric arrangement of the natural guide stars plays an important role in establishing AO performance (Flicker & Rigaut 2001). We assume nominal performance of Gemini MCAO and emphasize that both the areal coverage and PSF stability expected from MCAO are substantially larger than in the case with conventional (single-laser, single wavefront sensor) AO.

5.1. Figure of Merit

Any number of figures of merit can be devised for intercomparing the performance of various AO systems, but in this article we propose to use a figure of merit that captures the basic idea that real-world AO performance generally depends not only on image quality, but also on the variation of that image quality over the field of view. We therefore adopt the following figure of merit:

$$F = \frac{1}{\sigma_S^{0.25} \times (1 - \langle S \rangle)^{1.5}}, \tag{2}$$

where $\langle S \rangle$ is the average Strehl ratio achieved in the field of view, and σ_S is the rms variation in Strehl ratio over the field of view. In the present article our purpose is to understand the impact of tip-tilt stars, so we will be calculating Strehl ratios using simulation software that computes the distortion in the wavefront due to anisokinetism and assumes perfect correction for other aberrations in the wavefront. Our procedure for doing this will be described in the next section.

The distribution of F across the sky characterizes the performance of an AO system. The specific values of the exponents in our definition of F are chosen to weight the peak Strehl ratio at the expense of some uniformity in the value of the Strehl ratio over the field of view. However, uniformity in Strehl ratio is not completely deemphasized, and a guide star configuration resulting in a generally high, but strongly variable, Strehl ratio across the field of view will have a significantly lower value of F. None of main conclusions of this article are strongly dependent on the specific values of the exponents used in equation (2), as shown in Appendix B.

5.2. MCAO Observations in Existing and Proposed Fields

To investigate limitations in MCAO performance in various fields as a function of natural reference star magnitudes and configurations, we used the Gemini MCAO simulator (F. Rigaut 2009, private communication) to compute the distribution of the figure of merit F for ~1000 uniformly distributed pointings within several fields. As noted earlier, we wish to study the errors introduced into the corrected wavefront by a paucity of tip-tilt stars, so the Strehl ratio used in our analysis isolates the rms contribution to the distorted wavefront introduced by anisokinetism. In other words, the simulation assumes that all other contributions to the wavefront degradation are negligible, so if the tip-tilt correction were perfect, the Strehl ratio would be unity. In practice, of course, errors other than anisokinetism will contribute to the wavefront.[16] However, the point is that our analysis allows us to study *the best performance possible from the AO system*, limited only by the number of natural tip-tilt reference stars.

Each simulated pointing was $80'' \times 80''$ in size (appropriate to Gemini MCAO). We analyzed performance in the AODF, and for comparison with performance in unoptimized deep fields, we also examined ~1000 uniformly distributed positions in the COMBO-17 field 2 deep field and in the 1 deg^2 region of the CFHTLS wide field (W2). COMBO-17 field 2 (labeled as A 901 in Wolf et al. 2003) was chosen because it is the existing deep field with the highest star counts. We chose to include (a part of) the CFHTLS W2 field in this comparison because (1) it is located fairly close to the AODF, and (2) its star-count surface density is high. However, large portions of this $7° \times 7°$ field are contaminated with very bright stars.[17] In order to avoid those regions we performed our analysis in the $1° \times 1°$ subfield within CFHTLS W2 centered on R.A. $= 8^h42^m$, decl. $= -1°15'$, which has few very bright stars but an abundance of stars in the range suitable for tip-tilt correction.

To determine the optimal set of guide stars in each pointing, we looked for the best set of three stars with magnitudes in the range $13 < R < 16.5$ mag with distances between $40''$ and $60''$ from the field center (these distances are set by the patrol fields of pick-off mirrors in Gemini MCAO). As noted by Flicker & Rigaut (2001), the ideal geometry for these stars is an equilateral triangle, so we searched for three stars lying in the $40''$–$60''$ annulus whose interior angles were within $60° \pm 20°$ from each other. If we failed to find suitable stars, we then relaxed our criterion that the guide stars approximate equilateral triangles and simply searched for three stars defining a triangle with any set of side lengths. Where multiple triangles existed, we retained the one that gave the best value of F. When three stars

---

[16]The interested reader is directed to Table 2 of this World Wide Web page for a census of other contributions to the MCAO wavefront: http://www.gemini.edu/sciops/instruments/mcao?q=node/10749.

[17] See http://legacy.astro.utoronto.ca/Fields/images/w2.html.

in any geometry could not be found, we calculated MCAO performance with available stars, either singly or in pairs. In cases where no stars in the suitable magnitude range were found in the vicinity of our pointing, the value of F was set to zero.

The results from our investigation are shown in Figure 9, which compares the distribution and cumulative distribution functions of F for the AODF, with the corresponding distributions for the COMBO-17 field 2 and a 1 deg^2 region of the CFHTLS W2 field. The two panels of Figure 9 correspond to a limiting natural guide star magnitude of 16.5 mag in R band (corresponding to the anticipated limit for Gemini MCAO bright time observing). Although the limiting guide star magnitude will vary with lunation, the only difference in the case where the faintest natural guide stars is $R = 18.5$ mag (the ideal dark sky performance of Gemini MCAO) will be a higher number of pointings with low F.

The enormous benefits that emerge from observing in an AO-optimized field are obvious from even a cursory inspection of Figure 9, but it is worth discussing the figure in some detail. In analyzing this figure, we noted that even in our adaptive-opticsoptimized deep field (ID 8328, see Table 1), for bright time observing only about ~1% of the pointings in the field fall within triangles of guide stars that are approximately equilateral (as defined previously). However, if we allow any configuration of three suitably bright guide stars, sky coverage in the AODF is 55%. The $0 \leqslant F < 20$ range in this case covers the MCAO performance when less than three natural guide stars are available. If we assume dark time observing, the sky coverage is ~92% but the highest figure of merit still corresponds to the configurations

of brighter ($R \leqslant 16.5$) stars. In contrast to this, *none* of ~1000 uniformly distributed pointings in the COMBO-17 field 2 and only *one* pointing in the CFHTLS W2 subfield fell within equilateral triangles of natural guide for our simulated bright time conditions, and this fraction rises to only 0.2% (COMBO-17 field 2) and 1.2% (CFHTLS W2) at dark time. If the MCAO requirement is relaxed to allow any configuration of three NGSs, COMBO-17 field 2 coverage is 0.4% and 3.8% for bright and dark time observing conditions, respectively. Three AO-suitable stars with $R \leqslant 16.5$ forming a triangle were found in around 1.8% of the CFHTLS W2 pointings. If the magnitude limit is lowered to $R \leqslant 18.5$, CFHTLS W2 coverage for sets of three stars arranged in any type of triangle reaches 21%. For both COMBO-17 and CFHTLS W2, the most common figure-of-merit values that emerge ($0 \lesssim F \lesssim 20$) correspond to MCAO performance, with only one or two stars being natural tip-tilt stars. Thus, the low sky coverage in the COMBO-17 field 2 and CFHTLS W2 subfield results in the large spike in the first bin in Figure 9, with only a few (out of 1000) positions with high F producing a steep decline at $F \approx 20$. In contrast to this, the median value of F in the AO-optimized field is a factor of 3 higher than in COMBO-17 field 2 and CFHTLS W2, and a significant tail of F extends out to $F \sim 500$ (a factor of 3 better than the best F obtained in COMBO-17 field 2 and CFHTLS W2 subfield).

Figure 9 shows the superiority of the AODF over both COMBO-17 field 2 and CFHTLS W2 in terms of the figure of merit. The relation between the figure-of-merit values and the quantities that enter equation (2) (the average Strehl ratio
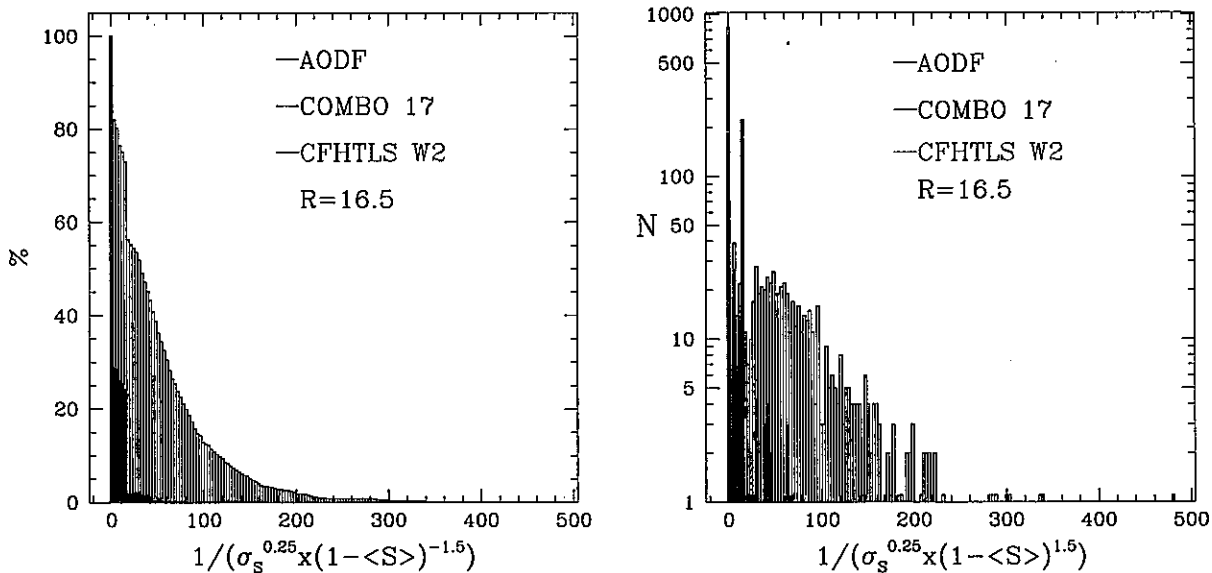

FIG. 9.—Cumulative distribution (*left*) and distribution (*right*) of our Strehl-ratio–related figure of merit for 55′ × 55′ AODF, COMBO-17 field 2, and the CFHTLS W2 subfield. Data points are binned according to their figure-of-merit value in three-unit-wide bins. The left-side vertical axis gives the percentage of field area with the figure-of-merit value equal to, or higher than, the corresponding bin's lower limit. In the right-side panel ordinate represents the number of pointings contained in each bin. Both panels correspond to a guide star magnitude limit of 16.5 mag in the R band (foreseen bright time limit for the Gemini MCAO system). See the text for details. See the electronic edition of the *PASP* for a color version of this figure.

and its rms variation over the field of view) is explored in Figure 10, where points are shaded according to their figure-of-merit values. (The reader is once again reminded that the Strehl ratios in our calculations take into account only the tip-tilt correction.) The dashed line in the left-hand panels denotes threshold value of the average Strehl ratio at which MCAO fails, i.e., when there are only one or two NGSs available. While ~70% of the AODF pointings with available NGSs have Strehl ratios above the MCAO threshold, for the COMBO-17 field 2 and the CFHTLS W2 that fraction is 3.8% and 8%, respectively. The right-hand panels show the distribution of Strehl ratios and corresponding variances for MCAO performance when the required geometry of guide stars is available. Figure 10 confirms that the figure of merit we have defined does rather nicely map onto fields with the combination of high average Strehl ratios *and* low rms variation in Strehl ratios over the $80'' \times 80''$ field of view. The third and fourth quartiles of the figure-of-merit distribution for the AODF (Fig. 10), which enclose Strehl ratios of $90\% < \langle S \rangle < 97\%$ and rms variations of

$1\% < \sigma_S < 6\%$, contain only 3% of the CFHTLS W2 pointings available for AO and 1.5% of the corresponding pointings within in the COMBO-17 field 2. This hugely better AO performance clearly illustrates the benefits of undertaking extragalactic AO observations in fields optimized for adaptive optics.

5.3. The AODF in the Era of Upcoming Methods and Instruments

Although the MCAO has been emphasized in the present article, other AO methods are in development especially for use with the 30 m class telescopes. These methods include multi-object adaptive optics (MOAO) and systems with faint IR tip-tilt sensors whose images are sharpened by the AO system. Future AO systems are expected to be less sensitive to the (bright) NGS surface density.

MOAO (Assémat et al. 2007) is a technique that allows simultaneous AO corrections for several small IFU target fields (typically 2–4″ in diameter, sufficient to map velocity fields of large spiral galaxies at $z \gtrsim 1$) within a wider field of view (FOV ~ 5–10′, driven by the surface density of line-emitting galaxies at $z \gtrsim 1$). Each IFU target field is corrected by a separate deformable mirror (DM) that provides AO correction along a given line of sight only (in contrast with MCAO systems that provide this correction across the whole FOV). Multiple NGSs are used for tomographic wavefront sensing (Ragazzoni et al. 2000), i.e., to probe the 3D phase perturbations in the atmosphere above the telescope primary aperture. A real-time control system then slices multiple columns through the mapped turbulent volume in the directions of all targets and applies a correcting signal to multiple independent DMs. The critical difference between MOAO and MCAO is that the former is an open-loop system where the wavefront sensors do not get any feedback
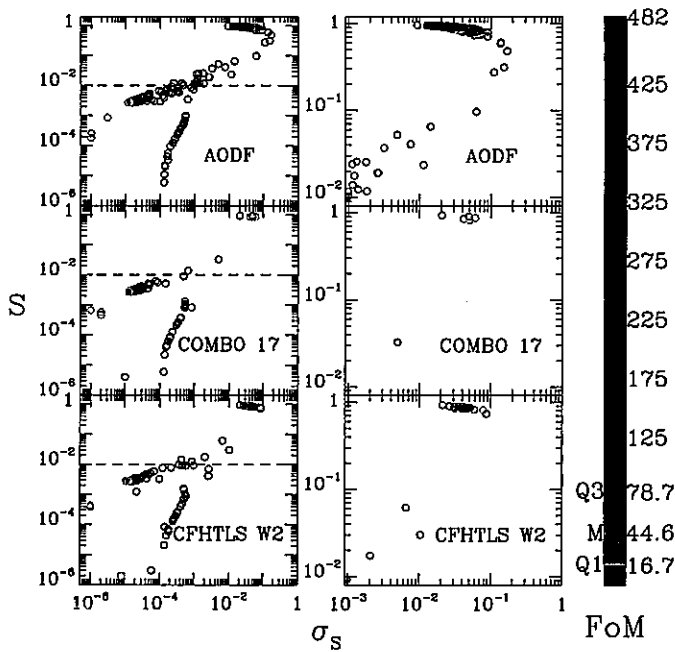

FIG. 10.—Strehl ratio as a function of its rms variance for pointings accessible to AO in AODF, COMBO-17 field 2, and CFHTLS W2 1 deg² subfield. Left-side panels display full range of values for Strehl ratio and its variance. The dashed line corresponds to MCAO failure for pointings where only one or two guide stars are available. The right-side panels show the range of Strehl ratios and related variances for pointings where MCAO is efficient (i.e., where at least one set of three AO-friendly stars forming a triangle is available). In each panel points are shaded according to figure-of-merit value (eq. [2]). Labels Q1, M, and Q3 represent the first quartile, median, and the third quartile of the figure-of-merit distribution across the AODF. All panels correspond to a guide star magnitude limit of 16.5 mag in the *R* band (the expected bright time magnitude limit for the Gemini MCAO system). See the electronic edition of the *PASP* for a color version of this figure.
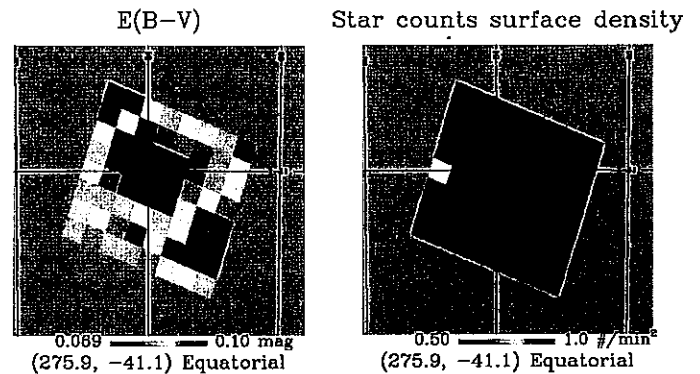

FIG. 11.—Extinction and star surface density maps of the $6.871'' \times 6.871''$ cells within the $55' \times 55'$ field with the highest mean star-count surface density of $\langle \Sigma_{sc} \rangle = 1.3$ arcmin⁻² (i.e., with 11,000 star-forming galaxies potentially observable with AO if the average number surface density of these objects is 3 arcmin⁻²). The field is centered at $\alpha = 18^h 23^m 39.53^s$ and $\delta = -41°6'44.3''$. The solid-line grid corresponds to the celestial coordinate system with R.A. [°] $= 360° - \alpha$ [°]. See the electronic edition of the *PASP* for a color version of this figure.

E(B−V)   Star counts surface density

0.041 ▬▬▬▬ ▬▬ 0.10 mag   0.50 ▬▬▬▬ ▬▬ 1.0 #/min
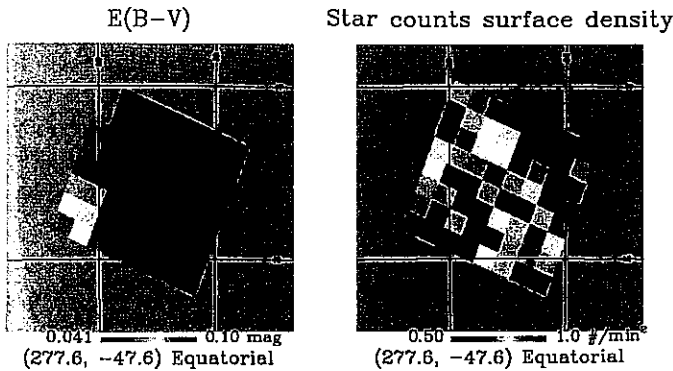(277.6, −47.6) Equatorial   (277.6, −47.6) Equatorial

FIG. 12.—Extinction and star surface density maps of the $6.871'' \times 6.871''$ cells within the $55' \times 55'$ field with the lowest reddening coefficient ($\langle E(B-V) \rangle = 0.053$ mag) but still containing more than 2500 possible guide stars (~5900 observable star-forming galaxies with number surface density of 3 arcmin^{-2}). The field is centered at $\alpha = 18^h30^m14.96^s$ and $\delta = -47°35'20.76''$. The solid-line grid corresponds to the celestial coordinate system with R.A. [°] $= 360° - \alpha$ [°]. See the electronic edition of the *PASP* for a color version of this figure.

E(B−V)   Star counts surface density

0.084 ▬▬▬ ▬▬ 0.10 mag   0.50 ▬▬▬▬ ▬▬ 1.0 #/min
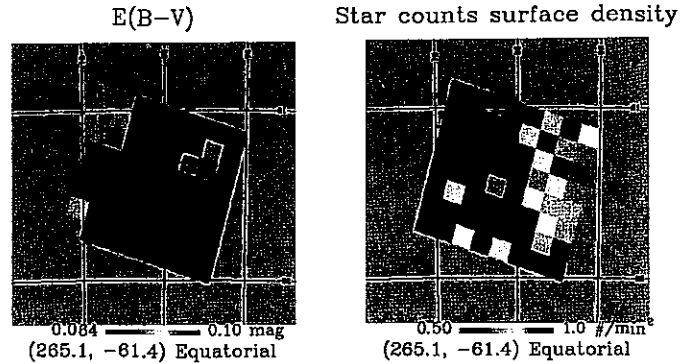(265.1, −61.4) Equatorial   (265.1, −61.4) Equatorial

FIG. 13.—Extinction and star surface density maps of the $6.871'' \times 6.871''$ cells within the $55' \times 55'$ field with the lowest standard deviation of $E(B-V)$) that translates into the smallest variation in dust content across the field. There are $\gtrsim 2350$ 13–16 mag stars suitable for AO guiding in the field corresponding to ~5600 observable star-forming galaxies with the number surface density of 3 arcmin^{-2}. The field is centered at $\alpha = 17^h40^m30.18^s$, $\delta = -61°25'54.54''$. The solid-line grid corresponds to the celestial coordinate system with R.A. [°] $= 360° - \alpha$ [°]. See the electronic edition of the *PASP* for a color version of this figure.

from DMs. In other words, the wavefront error is measured and corrected only once, and the accurate system calibration is essential.

While an advantage of open-loop MOAO is that it does not need a guide star for each target, the limiting magnitude of the NGS is set by the requirement for low system error level. Thus, even MOAO designed for the 30 m class telescopes will still need guide stars brighter than $R = 17$ mag. For example, an appropriate configuration for mapping turbulent atmospheric layers using the EAGLE MOAO system that is being developed for the E-ELT involves five NGSs with $R < 17$ mag in the $7.3'$ patrol FOV (Rousset et al. 2010). Based on the average star-count surface density, only one out of 55 existing deep fields mentioned earlier (COMBO-17) lies above (and very close to) this threshold. On the other hand, the number density of available NGSs in the AODF is six times higher than EAGLE MOAO requirements.

As was noted earlier, as the primary mirror of a telescope becomes larger, its sensitivity allows fainter stars to be used for wavefront sensing. AO systems on 30 m class telescope will give satisfying performance with a NGS magnitude limit of $R \approx 21$ mag (though the limiting magnitude will be lower in MOAO mode, as noted previously). We performed the same analysis as in previous section on the COMBO-17 field using the Gemini MCAO simulator and looked for stars arranged into triangles within magnitude range $13 < R < 21$, based on the USNO-B catalog (with limiting magnitude of $R = 22$; Monet et al. 2003). Although the sky coverage in this case is ~47%, only ~15% of these sets of three stars will provide Strehl ratio greater than 0.5. On the other hand, the sky coverage for high Strehl ratio values (i.e., guide stars arranged in equilateral or isosceles triangles) using MCAO system in the AODF is 100%.

Another advanced type of AO planned for 30 m class telescopes will utilize IR tip-tilt wavefront sensing. A major advantage of this approach is increased guide star density, since faint IR NGS images are sharpened by the AO system. For example, for the TMT Narrow-Field Infrared Adaptive Optics System (NFIRAOS) the probability of finding at least one tip-tilt star brighter than $J = 21$ mag is 95% at high Galactic latitude. However, at least three NGSs are still required to detect the effects of tilt anisoplanatism; the use of only one off-axis tip-tilt star would give blurred time-averaged images of the science objects. This condition lowers the sky coverage that NFIRAOS will achieve to 50% at high latitudes (Wang et al. 2008). Even with three guide stars one expects to get a continuum of performance. Fainter stars will force the system to run slower, which in turn leaves larger tip, tilt, and focus errors. Thus, although MCAO system on a 30 m class telescope will operate over much of the sky, an insufficient number of bright guide stars will impair imaging performance, as diffraction-limited cores will be blurred out by these tip/tilt/focus errors and the variation across the FOV will be increased. (IFU work will be less affected, because the ensquared energy loss in a spaxel a few times larger than the diffraction limit will be lower.) These types of systems will give the best results when used on a field densely populated with bright NGSs, where the AO is not pushing the boundaries of the control system. Finally, we note that AO using natural guide stars only (of magnitude ~12 and within ~15″ of the science object) is capable of achieving higher Strehls than MCAO, is easier to do, and removes all the complications of changing plate scales, cone effect, laser elongation, etc. A major benefit of doing AO in the proposed field is that it will allow much of the of the 30 m class telescope science to be done in NGS mode. For example, if an AO system, similar to EAGLE
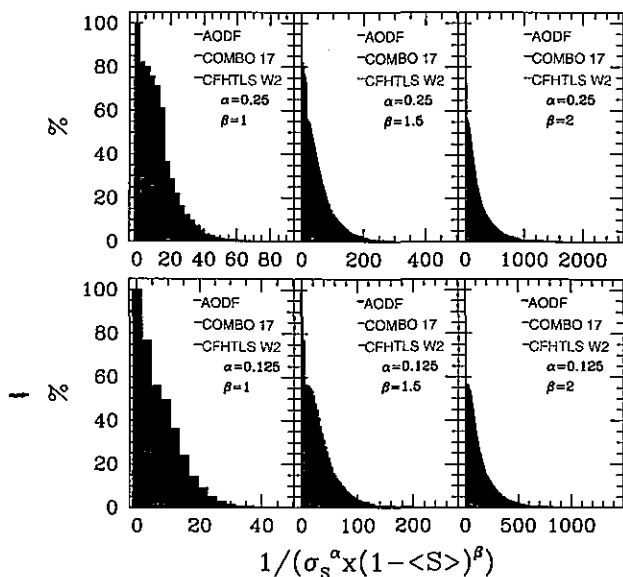
FIG. 14.—Cumulative distribution of our Strehl-related figure of merit for 55' ×55' AODF, COMBO-17 field, and the 1° × 1° subfield of CFHT W2. Data points are binned according to their figure-of-merit value in three-unit-wide bins. The vertical axis gives the percentage of field area with the figure-of-merit value equal to or higher than the corresponding bin's lower limit. In each panel the figure of merit is defined by different combinations of the two exponents (eq. [B1]). All panels correspond to a guide star magnitude limit of 16.5 mag in the R band (foreseen bright time limit for the Gemini MCAO system). See the electronic edition of the *PASP* for a color version of this figure.

FIG. 15.—Distribution of our Strehl-related figure of merit for 55' × 55' AODF, COMBO-17 field, and the 1° × 1° subfield of CFHT W2. Data points are binned according to their figure-of-merit value in three-unit-wide bins. Ordinate represents the number of pointings contained in an individual bin. In each panel the figure of merit is defined by different combinations of the two exponents (eq. [B1]). All panels correspond to a guide star magnitude limit of 16.5 mag in the R band (foreseen bright time limit for the Gemini MCAO system). See the electronic edition of the *PASP* for a color version of this figure.

MOAO, that uses only bright NGSs were employed in the AODF, sky coverage would be $\gtrsim 75\%$.

We conclude this section by noting that fields optimized for ground-based adaptive optics with 30 m class telescopes will not be made obsolete by upcoming space missions, such as *JWST* and Euclid/WFIRST (Wide Field Infrared Survey Telescope; both of which are 5–10 yr away in any case). Euclid/WFIRST will likely only operate in slitless spectroscopy mode, while *JWST* will be equipped with a microshutter array for simultaneous spectroscopy of ~100 sources and with an IFU for 3D spectroscopy, spanning the wavelength range of 1–5 μm (Gardner et al. 2006). However, the main point is that the future ground-based observations will still be undertaken at spatial resolutions that are factors of 5 and 15 times higher than the angular resolution of *JWST* and Euclid/WFIRST, respectively.

6. SUMMARY AND CONCLUSIONS

We have combed through stellar density and extinction maps to identify 67 low Galactic latitude fields with high star density, remarkably low extinction, relatively large area (1 deg², to mitigate the effects of cosmic variance), and an AO-friendly stellar mix of many $R = 13$–16.5 mag, but few <8 mag stars. These field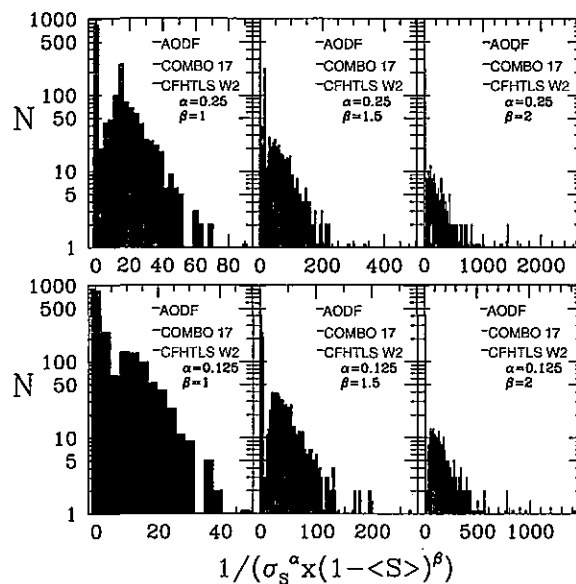s allow highly efficient adaptive optics to be undertaken in low-extinction extragalactic fields with minimal saturation and scattering. A comparison of these fields with existing deep fields reveals that while the number of guide stars per square arcminute is, on average, 15 times higher in the AO-friendly fields, the mean level of extinction is comparable with the more extincted existing deep fields.

By augmenting our analysis with some practical considerations (such as the desire for an equatorial field accessible from both hemispheres), we identify a single 1 deg² field (which we designate the adaptive optics deep field, or AODF) as being particularly promising for extragalactic AO work. This field is centered at R.A.: $7^h24^m3^s$, decl.: $-1°27'15''$. Analysis of galaxy counts in this field based on short observations of this AODF in g' and z' bands (using MegaCam on CFHT) confirm both the absence of extinction and the abundance of suitable tip-tilt stars the AODF. In fact, galaxy counts in this field closely follow the counts found in the CFHTLS Deep data set.

Simulations were undertaken to estimate the practical performance benefits of undertaking AO observations in the AODF. Our analysis shows enormous advantages emerge from undertaking AO observations in optimized fields such as the one described here. For example, for geometries of natural guide stars that produce spatially stable high Strehl ratio PSFs, dark time

sky coverage in the AODF is essentially 100% using the Gemini MCAO system, which is a factor of over 50 times higher than for most existing deep fields.

APPENDIX A

PROPERTIES OF SELECTED FIELDS

Figure 4 demonstrates how the set of $55' \times 55'$ fields that are most suitable for AO observations were selected. Amongst this set we chose our preferred field (the AODF) partly on the basis of accessibility to both hemispheres. Other fields may be equally (or even more) suitable if this criterion is relaxed. A field of obvious interest is the one with the highest star-count surface density. Table 1 shows that this field is located at $\alpha = 18^h21^m57.52^s$ and $\delta = -43°14'2.775''$. It is flagged with an open circle in Figures 4 and 8 and presented in more detail in Figure 11, where star-count surface density and extinction maps with finer sampling ($6.871'' \times 6.871''$) are used to bring out the features of individual cells within the field. The number of stars in this field is ~5000, corresponding to more than one star per arcminute squared.

Another property worth optimizing for is dust extinction, so it is interesting to look for fields with extraordinarily low extinction in Table 1. The field with the lowest reddening coefficient $E(B-V)$ is centered at $\alpha = 18^h30^m14.96^s$ and $\delta = -47°35'20.76''$ and is also flagged in Figures 4 and 8. A close-up view of its stellar surface density and reddening coefficient distribution is given in Figure 12. Although this field features lower extinction than some of already explored deep fields, the number of its potential AO guide stars is almost an order of magnitude higher than in the existing deep fields labeled in Figure 8.

Finally, it is interesting to consider fields with highly homogenous extinction. The third flagged field in Figures 4 and 8 is the one with the lowest value of standard deviation for $E(B-V)$ from Table 1 at $\alpha = 17^h40^m30.18^s$ and $\delta = -61°25'54.54''$. The properties of this field's $6.871'' \times 6.871''$ cells are given in Figure 13. Despite not having the highest number of AO-suitable stars ($\gtrsim 2350$ versus $\gtrsim 4600$) or the lowest dust extinction (its $\langle E(B-V) \rangle$ is ~35% higher than in the field with minimum extinction), this field may be interesting for certain studies in which reddening homogeneity is more important than other factors.

The higher-order statistical moments of star counts within subfields, along with proximity to other suitable areas, may be other factors worth considering when choosing fields. Whether the higher-order moments really matter depends on the specific science objectives of the observations. The skewness, γ_3, in the star-count surface density distribution might be worthwhile to consider in cases where one wishes to optimize for having a smaller number of fields with many NGSs. For example, $\gamma_3 < 0$ corresponds to the mass of distribution shifted toward higher values. For such fields there are many patches of very high star density. On the other hand, kurtosis in the $E(B-V)$ distribtuion, γ_4, could be important if one wishes to optimize a field for photo-z consistency. Fields with $\gamma_4 < 0$ have a less peaked distribution of $E(B-V)$, i.e., more uniform extinction. The area within dashed lines in Figure 4 contains the fields from three regions in the sky. When identifying the best AO field in each region (shaded arrows in Figures 4 and 5), we have taken into account all four moments of both star-count surface density and extinction distributions. In Figure 5 we present three moments—standard deviation, skewness, and kurtosis—for all 67 fields from Table 1 as functions of the mean star-count surface density (the most important factor for identifying AO-friendly fields).

APPENDIX B

THE FORM OF THE FIGURE OF MERIT

Our proposed figure of merit, given in equation (2), is useful for characterizing AO system performance, but there is considerable flexibility in choosing the values of the exponents in this equation. We chose exponents that strike a balance between emphasizing the importance of peak Strehl ratio in a field and emphasizing the uniformity of the Strehl ratio throughout the field. Other, equally valid, choices of these exponents could be made that strike a different balance. In order to investigate how different combinations of exponents in equation (B1) might influence our general conclu-sions, we have defined a more generic form of the figure of merit:

$$F = \frac{1}{\sigma_S^\alpha \times (1 - \langle S \rangle)^\beta},\qquad \text{(B1)}$$

where exponents α and β can take several values: $\alpha \in \{0.25, 0.125\}$ and $\beta \in \{1, 1.5, 2\}$. The maximum image quality (i.e., average Strehl ratio) is weighted by the β exponent. Constraints on the range of values for α are set so that

the high values of the figure of merit cannot coincide with extremely low values for both Strehl ratio and its variance.

The resulting distributions for all six possible combinations are given in Figures 14 and 15. In this figure we have examined and compared three fields: AODF, COMBO-17, and a $1° \times 1°$ subfield within CFHT W2. Of course, the range of values that the figure of merit can take is seen to depend rather strongly on the choice of exponents, but the important thing to note is that none of the distributions show major changes in shape or rela-

tive position for different combinations of α and β. Furthermore, the highest figures of merit in all six cases (for all three fields) correspond to the pointings with the highest average Strehl ratio ($\langle S \rangle > 90\%$) and relatively low variation of Strehl ratio across the $80'' \times 80''$ field of view ($\sigma_S \lesssim 2\%$). Since our analysis relies only on relative comparisons between different fields, our overall conclusions seem quite robust to the specific choices of the exponents.

REFERENCES

Abazajian, K. N., et al. 2009, ApJS, 182, 543

Alcalá, J. M., et al. 2004, A&A, 428, 339

Arnouts, S., et al. 2007, A&A, 476, 137

Assémat, F., Gendron, E., & Hammer, F. 2007, MNRAS, 376, 287

Bell, E. F., et al. 2004, ApJ, 608, 752

Bertin, E., et al. 2002, ASP Conf. Proc. 281, Astronomical Data Analysis Software and Systems XI, (San Francisco: ASP), 228

Bessell, M. S. 1979, PASP, 91, 589

Bonaccini, D., et al. 1999, Messenger, 98, 8

Bournaud, F., Elmegreen, B. G., & Elmegreen, D. M. 2007, ApJ, 670, 237

Bouwens, R. J., et al. 2009, ApJ, 705, 936

———. 2010, ApJ, submitted (arXiv:1003.1706)

Cooper, M. C., et al. 2008, MNRAS, 383, 1058

Coupon, J., et al. 2009, A&A, 500, 981

Cowie, L. L., Hu, E. M., & Songaila, A. 1995, AJ, 110, 1576

Davies, R., et al. 2008, Messenger, 131, 7

Davis, M., et al. 2007, ApJ, 660, L1

Dickinson, M., et al. 2003, in ESO Astrophys. Symp., The Mass of Galaxies at Low and High Redshift, ed. R. Bender, & A. Renzini (Berlin: Springer), 324

Driver, S. P., & Robotham, A. S. G. 2010, MNRAS, accepted (arXiv: 1005.2538)

Egami, E., et al. 2004, ApJS, 154, 130

Eikenberry, S. S., et al. 2004, Proc. SPIE, 5492, 1196

Ellerbroek, B. L., & Tyler, D. W. 1998, PASP, 110, 165

Ellerbroek, B. L., et al. 2003, Proc. SPIE, 4839, 55

Ellis, R. 1997, ARA&A, 35, 389

Epinat, B., et al. 2009, A&A, 504, 789

Erb, D. K., et al. 2006, ApJ, 646, 107

Flicker, R., & Rigaut, F. 2001, in ESO Conf. Proc. 58, Beyond Conventional Adaptive Optics, (Garching: ESO), 377

Flores, H., et al. 2006, A&A, 455, 107

Förster-Schreiber, N. M., et al. 2009, ApJ, 706, 1364

Fukugita, M., et al. 2004, AJ, 127, 3155

Gardner, et al. 2006, Space Sci. Rev., 123, 485

Górski, K. M., et al. 2005, ApJ, 622, 759

Green, A. W., et al. 2010, Nature, 467, 684

Labbé, I., et al. 2003, AJ, 125, 1107

Lai, O., et al. 2008, Proc. SPIE, 7015, 70154H

Law, D. R., et al. 2009, ApJ, 697, 2057

Mannucci, F. 2007, Poster at Astronomy with Laser Guide Star Adaptive Optics (Schloss Ringberg), http://www.mpia-hd.mpg.de/PARSEC/Ring2007/TalksPostersPDF/Tuesday/Highz_FilippoMannucci.pdf

McGregor, P., et al. 2004, Proc. SPIE, 5492, 1033

Monet, D. G., et al. 2003, AJ, 125, 984

Moustakas, L. A., & Somerville, R. S. 2002, ApJ, 577, 1

Ono, Y., et al. 2010, MNRAS, 402, 1580

Queyrel, J., et al. 2009, A&A, 506, 681

Ragazzoni, R., Marchetti, E., & Valente, G. 2000, Nature, 403, 54

Rigaut, F. J., et al. 2000, Proc. SPIE, 4007, 1022

Rigaut, F., & Gendron, E. 1992, A&A, 261, 667

Rix, H.-W., et al. 1997, MNRAS, 285, 779

———. 2004, ApJS, 152, 163

Roggemann, M. C., & Welsh, B. 1996, Imaging through Turbulence (Boca Raton: CRC)

Rousset, G., et al. 2010, in 1st AO4ELT Conf., Adaptative Optics for Extremely Large Telescopes, ed. Y. Clnet, J.-M. Conan, T. Fusco, & G. Rousset (02008; Paris: EDP Sciences)

Schlegel, D. J., et al. 1998, ApJ, 500, 525

Scoville, N., et al. 2007, ApJS, 172, 1

Shim, H., et al. 2009, ApJ, 696, 785

Trenti, M., & Stiavelli, M. 2008, ApJ, 676, 767

van Dokkum, P. G., et al. 2004, ApJ, 611, 703

Villar, V., et al. 2008, ApJ, 677, 169

Wang, L., et al. 2008, Proc. SPIE, 7015, 163

Wolf, C., et al. 2003, A&A, 401, 73

Yasuda, N., et al. 2007, AJ, 134, 698

Yee, H. K. C., et al. 2000, ApJS, 129, 475

Zacharias, N., et al. 2004, AJ, 127, 3043